JCTC Journal of Chemical Theory and Computation

Article

pubs.acs.org/JCTC

Simulating Valence-to-Core X-ray Emission Spectroscopy of Transition Metal Complexes with Time-Dependent Density Functional Theory

Yu Zhang,*[,†] Shaul Mukamel,*[,†] Munira Khalil,[‡] and Niranjan Govind*[,¶]

[†]Department of Chemistry, University of California, Irvine, California 92697, United States

[‡]Department of Chemistry, University of Washington, Seattle, Washington 98195, United States

[¶]Environmental Molecular Sciences Laboratory, Pacific Northwest National Laboratory, P.O. Box 999, Richland, Washington 99352, United States

Supporting Information

ABSTRACT: Valence-to-core (VtC) X-ray emission spectroscopy (XES) has emerged as a powerful technique for the structural characterization of complex organometallic compounds in realistic environments. Since the spectrum represents electronic transitions from the ligand molecular orbitals to the core holes of the metal centers, the approach is more chemically sensitive to the metal−ligand bonding character compared with conventional X-ray absorption techniques. In this paper we study how linear-response time-dependent density functional theory (LR-TDDFT) can be harnessed to simulate K-edge VtC X-ray emission spectra reliably. LR-TDDFT allows one to go beyond the single-particle picture that has been extensively used to simulate VtC-XES. We consider seven low- and high-spin model complexes involving chromium, manganese, and iron transition metal centers. Our results are in good agreement with experiment.

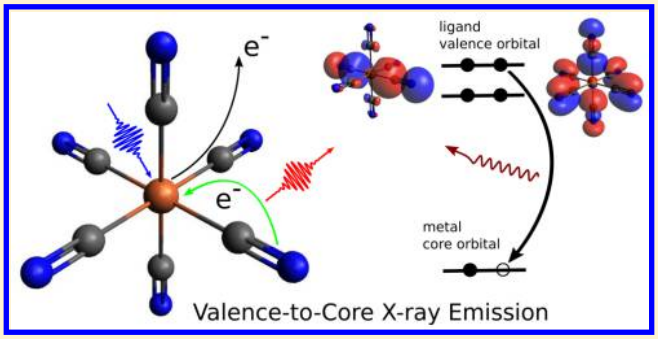

1. INTRODUCTION

Understanding the local chemical environment, electronic structure, and geometric configuration of metal centers in transition metal (TM) complexes and materials is essential to catalyst design, magnetism, photochemical energy conversion, and several other applications. X-ray spectroscopic methods are ideal for this purpose because of their element selectivity. Ultrafast X-ray absorption spectroscopies (XAS), including X-ray absorption near edge (XANES) and extended X-ray absorption fine structure (EXAFS) spectroscopies, have gained a lot of success in characterizing the geometric and electronic structures of stable or transient TM complex species.[1,2] However, XANES can only indirectly probe metal−ligand interactions through the unoccupied valence orbitals, and traditional EXAFS suffers from a lack of chemical sensitivity for light atoms, such as carbon, nitrogen, and oxygen that are in close proximity to a metal center.

These limitations can be overcome by the valence-to-core X-ray emission spectroscopy (VtC-XES) technique.[3,4] In a typical X-ray emission spectroscopy (XES) experiment, first a core hole state is created through X-ray photoionization or radioactive electron capture decay,[5] then the fluorescence transitions from higher occupied core or valence orbitals are recorded as emission lines. VtC-XES lines lie in the high energy tail of an X-ray emission spectrum. They represent the transitions from the valence orbitals to the empty core orbital (usually the 1*s* orbital of the metal center). Because of the dipole selection rule, transitions from metal *d* molecular orbitals (MOs) to the metal 1*s* MOs are very weak, and the observed VtC-XES features mainly involve transitions from ligand *s* and *p* MOs to the metal 1*s* core hole. Since the ligand *s* and *p* orbitals play a dominant role in the chemical bonding between the metal centers and ligands, VtC-XES spectroscopy can shed light on the metal−ligand bonding.

Traditionally, VtC-XES features are grouped into two categories labeled as Kβ'' and K$\beta_{2,5}$, respectively. The Kβ'' peaks are weaker and lower in energy, while the K$\beta_{2,5}$ peaks are stronger and higher in energy as shown in Figure 1. The Kβ'' peaks have long been assigned to transitions involving ligand *s* MOs, while the K$\beta_{2,5}$ peaks have been assigned to transitions involving ligand *p* MOs.[7] The energy splittings between the Kβ'' and K$\beta_{2,5}$ peaks approximately represent the binding energy differences between the ligand *s* and *p* orbitals, respectively, and can be used for ligand identification.[8,9] Broadly speaking, the normalized intensities of Kβ'' peaks depend on the ligand−metal distance in an exponential fashion,[8] which provides a qualitative tool to study the local structure around the metal center. The intensities of VtC-XES features can also be used to reveal the valence orbital

Received: August 7, 2015
Published: November 9, 2015

DOI: 10.1021/acs.jctc.5b00763
J. Chem. Theory Comput. 2015, 11, 5804−5809

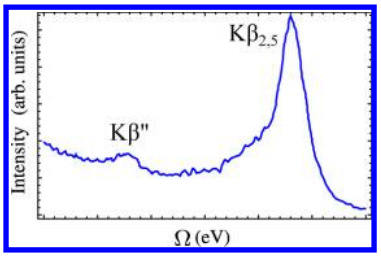

Figure 1. A typical VtC X-ray emission spectrum showing Kβ'' and K$\beta_{2,5}$ features (experimental spectrum of $[Cr^{III}(NH_3)_6]^{3+}$ adapted from ref 6). The baseline of the spectrum is not horizontal because the exponential tail of the strong Kβ mainline has not been subtracted.

compositions.[10−12] As a hard X-ray spectroscopy technique, VtC-XES has the ability to probe samples in a variety of environments including *in situ* studies.[13] The information from VtC-XES spectroscopy is similar to that from valence-band X-ray photoelectron spectroscopy (XPS).[5] However, in VtC-XES, only the MOs localized around the metal center are probed, and ultrahigh vacuum experimental conditions are not required. The VtC-XES features are typically weak (≈100 times weaker than the Kβ mainline), and a large Kβ mainline tail has to be subtracted in order to reveal a clean VtC-XES spectrum, both of which pose challenges from an experimental standpoint. However, the rapid development of new state-of-the-art intense synchrotron X-ray lasers has greatly improved the quality of VtC-XES spectroscopy.[3,4] In short, VtC-XES provides a complementary and powerful spectroscopic approach to characterize TM complexes and materials in realistic environments.

We focus on VtC-XES calculations using Gaussian basis sets in this paper. For a broader discussion on theoretical methods for XES simulations, see the recent review by Rovezzi and Glatzel[14] and references therein. In addition to the multiple scattering real-space Green's function approach[15] which has been successfully used to study VtC-XES of solid state compounds,[16−18] over the past few years there have been many theoretical studies[6,9−12,19−21] on VtC-XES of molecular complexes using a single-particle density functional theory (DFT) based approach. In the latter, the initial core hole and final valence ionized states are both represented by single Slater determinants constructed with Kohn−Sham (KS) orbitals from ground state DFT calculations. Within this approximation, the emission intensities are proportional to the transition dipole matrix elements between the two aforementioned Kohn−Sham orbitals, and the emission energies are just the energy differences between the initial and final states. However, there are several limitations with this approach. First, it neglects orbital relaxation during the emission process. Fortunately the core hole potential is largely screened from the point of view of the ligand orbitals involved in VtC X-ray emission processes. For the X-ray ionization which triggers the subsequent emission, the leaving electron is ignored, and multichannel effects in the X-ray emission are also omitted in the single-particle DFT treatment. In addition, the emission process involving many orbital pairs with significant contributions cannot be described within a single-particle framework. Finally, many-body effects from shake-up states generated from the X-ray ionization process cannot be captured with this approach.

Within the single-particle theory framework, the initial core hole state can be modeled with the Z+1 or equivalent core hole (ECH) approximation.[19,22,23] Other core hole approximations[24] include the full core hole (FCH),[25−27] half core hole (HCH),[28,29] and excited core hole (XCH)[30] approaches. We have previously combined XCH with LR-TDDFT[31−33] to study double core excited states.[34] Here, we utilize the protocol proposed by Besley and co-workers[35] to simulate VtC-XES spectra. We have applied this approach to calculate the K-edge VtC-XES spectra of seven model TM (Cr, Mn, Fe) complexes and compare the results with experiment.

The rest of the paper is organized as follows: in the next section we outline the model systems and the computational details followed by a discussion of our results, and finally we summarize our findings.

2. SYSTEMS

We have chosen the following Cr, Mn, and Fe model TM complexes: $[Cr^{III}(NH_3)_6]^{3+}$, $[Cr^{0}(CO)_6]$; $Mn^{II}(H_2O)_6]^{2+}$, $[Mn^{II}(CN)_5N]^{3-}$; $[Fe^{II}(CN)_6]^{4-}$, $[Fe^{III}(CN)_6]^{3-}$, and $[Fe^{II}(CN)_5(NO)]^{2-}$. We studied the dominant spin states of these complexes, that is, the high-spin quartet for $[Cr^{III}(NH_3)_6]^{3+}$, the low-spin singlet for $[Cr^{0}(CO)_6]$, the high-spin sextet for $Mn^{II}(H_2O)_6]^{2+}$, the low-spin doublet for $[Mn^{II}(CN)_5N]^{3-}$, the low-spin singlet for $[Fe^{II}(CN)_6]^{4-}$, the low-spin doublet for $[Fe^{III}(CN)_6]^{3-}$, and the low-spin singlet for $[Fe^{II}(CN)_5(NO)]^{2-}$. All structures are provided in the Supporting Information.

3. COMPUTATIONAL DETAILS

LR-TDDFT[31−33] has the ability to treat many types of linear and nonlinear X-ray spectroscopies such as XANES, XES, and stimulated X-ray Raman spectroscopy (SXRS)[35−42] within the same theory framework. Many of these spectroscopies go beyond the reach of single-particle DFT. In this paper we utilize LR-TDDFT within the Tamm-Dancoff approximation (TDA)[43] to simulate VtC X-ray emission. All calculations were performed with a development version of the NWChem package[44] which includes higher-order contributions to the oscillator strengths. The optimized geometry of $[Mn^{II}(CN)_5N]^{3-}$ was taken from ref 20, and the optimized geometries of $[Cr^{III}(NH_3)_6]^{3+}$ and $[Cr^{0}(CO)_6]$ were taken from ref 6. Geometry optimizations for the remaining structures were performed with the B3LYP exchange-correlation functional[45,46] and def2-TZVP[47] basis sets without symmetry constraints. The conductor like screening (COSMO) model[48] was used to simulate the effect of the solvent (water, ϵ = 78.4). All VtC-XES calculations on the optimized geometries were performed with the B3LYP exchange-correlation functional and Sapporo-TZP-2012[49] and 6-311G**[50,51] basis sets for the TM centers and ligand atoms, respectively.

Our VtC-XES simulation protocol is as follows: first a neutral ground state calculation is performed, an FCH ionized state is then obtained self-consistently where the 1*s* core orbital of the TM center is swapped with a virtual orbital, then a LR-TDDFT calculation within the TDA is performed with the FCH ionized state as reference. To prevent core hole collapse during the FCH calculation, we have employed the maximum overlap constraint as implemented in NWChem.[52,53] Unlike XANES calculations,[36−41] a restricted excitation window is not necessary as the VtC-XES features appear as negative eigenvalues at the bottom of the spectrum. The final spectra are obtained by taking the absolute value of the negative eigenvalues. For the open-shell species, ionization of both α and β core electrons are considered. The final spectrum is the

DOI: 10.1021/acs.jctc.5b00763
J. Chem. Theory Comput. 2015, 11, 5804−5809

sum of spectra from both ionization modes. Energy shifts are applied to match experimental spectra (see figure captions for the shift values). All spectra were Lorentzian broadened by 1.5 eV. Spin−orbit coupling (SOC) effects are not included in our current implementation, but these are more likely to affect the Kβ mainline compared with the VtC-XES, which involves transitions from the ligand *s* and *p* orbitals, where these effects are small (≈0.2 eV), to the 1*s* orbitals of the TM centers. In addition, this small spin−orbit splitting is much smaller than the intrinsic lifetime widths (>1.0 eV) of the core holes we have studied in this paper. A sample input file for the VtC-XES calculations is provided in the Supporting Information.

It is known that LR-TDDFT with an unrestricted Kohn−Sham reference can lead to spin-contamination. Casida et al.[54] have suggested using the difference of S^2 values between the excited and reference states (i.e., ΔS^2) as an indicator for spin contamination.[55] A large difference means the corresponding excited state is unphysical. In our VtC-XES simulations, we find small ΔS^2 values (<0.1).

4. RESULTS

4.1. $[Fe^{II}(CN)_6]^{4-}$. From Figure 2 we can see that the simulation reproduces the experimental spectrum. We note that

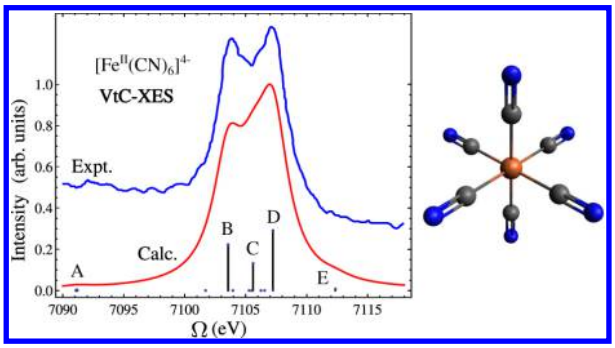

Figure 2. Experimental and simulated VtC-XES spectra of $[Fe^{II}(CN)_6]^{4-}$. Simulated results have been red-shifted by 20.5 eV to match experiment.[21] The molecular structure is shown on the right. Color code: N (blue), Fe (orange), C (gray).

all experimental spectra in this paper contain the Kβ mainline decay tails except for the $[Mn^{II}(H_2O)_6]^{2+}$ spectrum, hence the low energy features appear stronger compared with the simulated results. Representative groups of features are labeled as A−E in the figure. Our calculations indicate that the strongest feature D around 7107.2 eV corresponds to electronic transitions between the carbon *sp* hybrid orbitals, the CN π orbitals, and the Fe 1*s* core hole. Feature C around 7105.6 eV represents the de-excitation involving the nitrogen *sp* hybrid orbitals and the CN π orbitals, and feature B around 7103.6 eV is mainly related to the carbon and nitrogen 2*s* orbitals. Features B, C, and D together give the strong double peak profile characteristic of VtC-XES spectra of cyanometalates. Similar strong double peaks are also seen in the experimental and simulated spectra of $[Fe^{III}(CN)_6]^{3-}$, $[Fe^{II}(CN)_5(NO)]^{2-}$, and $[Mn^{II}(CN)_5N]^{3-}$, respectively. Feature A can be assigned to transitions from the nitrogen 2*s* orbitals to the Fe 1*s* core-hole, and they are too weak to be seen clearly in the experimental spectrum. Feature E corresponds to Fe 3*d* and CN $\pi \rightarrow$ 1*s* transitions. They are quadrupolar in nature and hence very weak. Calculated and experimental peak positions and plots of representative relevant ligand orbitals with major contributions to the VtC-XES features are presented in the Supporting Information for all systems studied.

4.2. $[Fe^{III}(CN)_6]^{3-}$. We then studied the $[Fe^{III}(CN)_6]^{3-}$ complex. From Figure 3 we see a similar spectrum to the

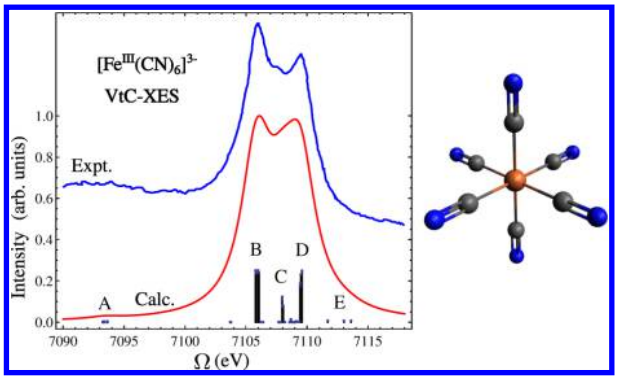

Figure 3. Experimental and simulated VtC-XES spectra of $[Fe^{III}(CN)_6]^{3-}$. Simulated results have been red-shifted by 20.6 eV to match experiment.[21] The molecular structure is shown on the right. Color code: N (blue), Fe (orange), C (gray).

$[Fe^{II}(CN)_6]^{4-}$ complex described earlier. Despite the overall similarity, the strong features B (7105.8−7106.1 eV), C (≈7108.0 eV), and D (7109.4−7109.6 eV) are blue-shifted by ≈2.4 eV, which represents the effect of different oxidation states of the TM center, Fe(II) vs Fe(III). All features have similar character as their $[Fe^{II}(CN)_6]^{4-}$ counterparts (see the MO plots in the Supporting Information).

4.3. $[Fe^{II}(CN)_5(NO)]^{2-}$. Compared with $[Fe^{II}(CN)_6]^{4-}$, $[Fe^{II}(CN)_5(NO)]^{2-}$ has one $(CN)^-$ ligand replaced with $(NO)^+$, leading to changes in the VtC-XES spectrum. As shown in Figure 4, the strong double peaks still exist (D, E, F features),

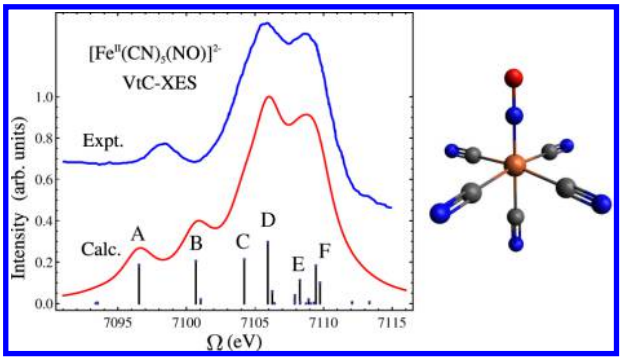

Figure 4. Experimental and simulated VtC-XES spectra of $[Fe^{II}(CN)_5(NO)]^{2-}$. Simulated results have been red-shifted by 20.5 eV to match experiment.[21] The molecular structure is shown on the right. Color code: N (blue), Fe (orange), C (gray), O (red).

but both the experimental and the simulated features in the low energy region are much stronger than those in the $[Fe^{II}(CN)_6]^{4-}$ system. There is only one broad peak in the low energy region (7096.0−7101.0 eV) experimentally, while simulations show two features (A and B) in the same energy range. The experiment was performed in the solid state, while our simulations are performed in solution, which may account for the differences. These extra peaks have also been reported by March and co-workers[21] in their single-particle based DFT simulations in solution. Solid state simulations should help resolve this discrepancy. MO analysis shows that the A feature

DOI: 10.1021/acs.jctc.5b00763
J. Chem. Theory Comput. 2015, 11, 5804−5809

originates from transitions between the nitrogen and oxygen 2*s* orbitals of the $(NO)^+$ ligand and the Fe 1*s* core hole, and the B feature is related to oxygen and nitrogen 2*p* orbitals of $(NO)^+$ (see the Supporting Information). Since the $(NO)^+$ ligand directly coordinates the Fe center with the nitrogen atom, the Fe−N distance is much shorter than those in $[Fe^{II}(CN)_6]^{4-}$, which explains why the A feature in Figure 4 is much stronger than the A feature in Figure 2. The C feature mostly represents de-excitations from the carbon 2*s* orbitals. Since the C and D features are close, they combine to form a strong broad double peak. Features D, E, and F in Figure 4 are similar to the B, C, and D features in Figure 2, respectively. Comparing the spectra of the two species, one can see that the small ligand modification can result in large changes in specific regions of VtC-XES spectra, highlighting the sensitivity of approach to the local chemical environment of TM metal centers.

4.4. $[Mn^{II}(CN)_5N]^{3-}$. Furthermore, we studied the manganese cyanide complex $[Mn^{II}(CN)_5N]^{3-}$. Not surprisingly, for a different TM center we still see the strong double peaks (B, C, and D features in Figure 5) as those in Figures 2−4. B, C, and D features in Figure 5 have similar character to B, C, and D features in Figure 2, respectively. Similarly, the A feature in Figure 5 represents transitions from the 2*s* orbital of the nitrogen atom directly coordinating to Mn, and the increased intensity is due to its short distance to the metal center. This suggests that the intensities of characteristic VtC-XES peaks can be used to estimate the distance between the target atom and the metal center.

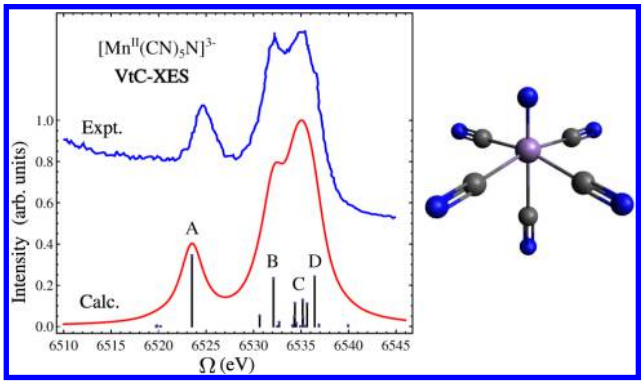

Figure 5. Experimental and simulated VtC-XES spectra of $[Mn^{II}(CN)_5N]^{3-}$. Simulated results have been red-shifted 28.0 eV to match experiment.[20] The molecular structure is shown on the right. Color code: N (blue), Mn (purple), C (gray).

4.5. $[Mn^{II}(H_2O)_6]^{2+}$. For the high-spin Mn complex $[Mn^{II}(H_2O)_6]^{2+}$, the simulated VtC-XES spectrum matches experiment almost perfectly (see Figure 6). Here B, C, and D features consist of transitions from linear combinations of oxygen 2*p* orbitals to the Mn 1*s* core hole, and the A feature is composed of transitions involving the oxygen 2*s* orbitals. The experimental spectrum shows a strong broad peak and some weak features in the low energy region. The asymmetric shape of the strong peak indicates the existence of adjacent weak shoulders at both low and high energies in the region around the main peak. Our simulated spectrum clearly captures these weak features (B and D features in Figure 6), while the D feature is absent in previously reported calculations[19] based on the single-particle DFT method described earlier, leading to an incorrect line shape of the strong peak. Careful MO analysis of the TDDFT calculations shows that the D feature corresponds

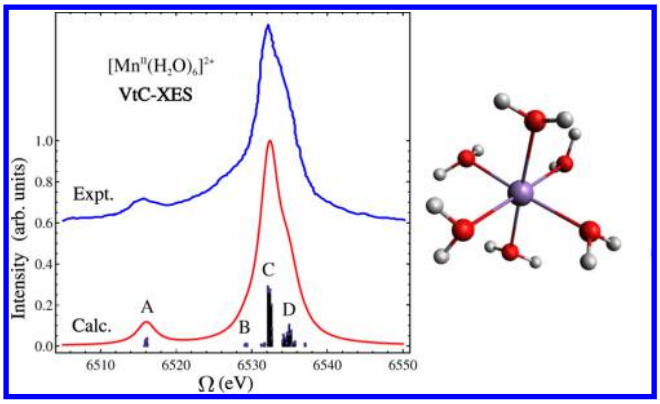

Figure 6. Experimental and simulated VtC-XES spectra of $[Mn^{II}(H_2O)_6]^{2+}$. Simulated results have been red-shifted by 30.4 eV to match experiment.[19] The molecular structure is shown on the right. Color code: O (red), Mn (purple), H (white).

to transitions which have strong multideterminant character and are thus naturally captured by our approach.

4.6. $[Cr^{III}(NH_3)_6]^{3+}$. Our simulations excellently reproduce the experimental VtC-XES profile of the high-spin Cr complex $[Cr^{III}(NH_3)_6]^{3+}$. In Figure 7 the A feature represents transitions from the nitrogen 2*s* orbitals, and B and C features represent transitions from linear combinations of nitrogen 2*p* orbitals. The weak shoulder B feature in the experiment is also well captured.

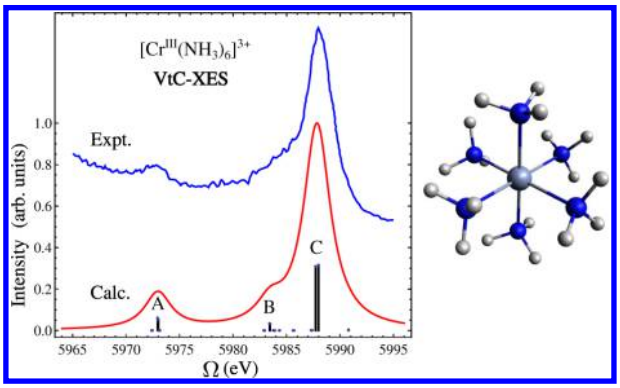

Figure 7. Experimental and simulated VtC-XES spectra of $[Cr^{III}(NH_3)_6]^{3+}$. Simulated results have been red-shifted by 32.2 eV to match experiment.[6] The molecular structure is shown on the right. Color code: N (blue), Cr (light blue) and H (white).

4.7. $[Cr^0(CO)_6]$. The agreement between the simulated and experimental VtC-XES spectra of the low-spin Cr complex $[Cr^0(CO)_6]$ is also very good. As stated before, the relative intensity of the shoulder in the experimental spectrum can be reduced if the Kβ mainline decay tail is subtracted. In Figure 8, the A feature involves transitions from carbon and oxygen 2*s* orbitals, the B feature involves transitions from oxygen 2*p* orbitals, and the C feature involves transitions from carbon 2*p* orbitals. Transitions that are mainly from the oxygen 2*s* orbitals are too weak to observe since the oxygen atoms do not directly coordinate to the Cr center.

5. CONCLUSIONS

In this paper we have demonstrated how LR-TDDFT within the TDA based on a FCH ionized reference state can be used to simulate K-edge VtC-XES spectra reliably. In contrast with

DOI: 10.1021/acs.jctc.5b00763
J. Chem. Theory Comput. 2015, 11, 5804−5809

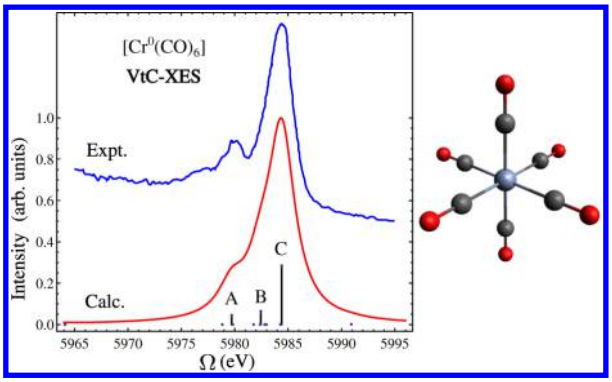

Figure 8. Experimental and simulated VtC-XES spectra of $[Cr^0(CO)_6]$. Simulated results have been red-shifted by 31.3 eV to match experiment.[6] The molecular structure is shown on the right of the spectra. Color code: O (red), Cr (light blue), C (gray).

the single-particle DFT approach, which provides a reliable description of single configuration dominant VtC X-ray emission processes,[6,9−12,19−21] our approach is well-suited to describe emission processes with multiconfigurational character. This is especially seen in the simulation of the VtC-XES spectra of the $[Mn^{II}(H_2O)_6]^{2+}$ system. In order to check how the reference MOs affect the simulated VtC-XES results, we also run TDDFT calculations with the unrelaxed ground state MOs to obtain the VtC-XES features. Results show that this choice leads to worse energy differences between VtC-XES features, compared to the simulated results with core-hole-relaxed MOs and experiment. An example of such comparison for the Mn(II) water complex can be found in the Supporting Information. An open question with our approach is the ability to simulate shake-up states. If these states can be described with single Slater determinants, we should be able to include their effects in the VtC-XES spectra with the protocol described in this paper. Further systematic benchmark calculations are needed to assess this.

■ ASSOCIATED CONTENT

Supporting Information

The Supporting Information is available free of charge on the ACS Publications website at DOI: 10.1021/acs.jctc.5b00763.

A sample NWChem input file for VtC-XES calculations, molecular coordinates, calculated peak positions and oscillator strengths together with the corresponding experimental results, and representative molecular orbitals involved in the important VtC X-ray emission processes of all studied species, comparison of simulated VtC-XES spectra with the relaxed and unrelaxed MOs of the Mn(II) water complex (PDF)

■ AUTHOR INFORMATION

Corresponding Authors

*E-mail: yuz10@uci.edu.
*E-mail: smukamel@uci.edu.
*E-mail: niri.govind@pnnl.gov.

Notes

The authors declare no competing financial interest.

■ ACKNOWLEDGMENTS

This material is based upon work supported by the U.S. Department of Energy, Office of Science, Office of Basic Energy Sciences under Award Numbers DE-SC0012450 (Y.Z., S.M., M.K.), and KC030102066418 (N.G.). This research was performed using EMSL, a DOE Office of Science User Facility sponsored by the Office of Biological and Environmental Research and located at PNNL. PNNL is operated by Battelle Memorial Institute for the United States Department of Energy under DOE contract number DE-AC05-76RL1830. The research also benefited from resources provided by the National Energy Research Scientific Computing Center (NERSC), a DOE Office of Science User Facility supported by the Office of Science of the U.S. Department of Energy under Contract No. DE-AC02-05CH11231.

■ REFERENCES

(1) Milne, C. J.; Penfold, T. J.; Chergui, M. *Coord. Chem. Rev.* **2014**, *277−278*, 44−68.
(2) Chen, L. X.; Zhang, X.; Shelby, M. L. *Chem. Sci.* **2014**, *5*, 4136−4152.
(3) Gallo, E.; Glatzel, P. *Adv. Mater.* **2014**, *26*, 7730−7746.
(4) Bauer, M. *Phys. Chem. Chem. Phys.* **2014**, *16*, 13827−13837.
(5) Glatzel, P.; Bergmann, U. *Coord. Chem. Rev.* **2005**, *249*, 65−95.
(6) MacMillan, S. N.; Walroth, R. C.; Perry, D. M.; Morsing, T. J.; Lancaster, K. M. *Inorg. Chem.* **2015**, *54*, 205−214.
(7) Best, P. E. *J. Chem. Phys.* **1966**, *44*, 3248−3253.
(8) Bergmann, U.; Horne, C. R.; Collins, T. J.; Workman, J.; Cramer, S. P. *Chem. Phys. Lett.* **1999**, *302*, 119−124.
(9) Swarbrick, J. C.; Kvashnin, Y.; Schulte, K.; Seenivasan, K.; Lamberti, C.; Glatzel, P. *Inorg. Chem.* **2010**, *49*, 8323−8332.
(10) Lee, N.; Petrenko, T.; Bergmann, U.; Neese, F.; DeBeer, S. *J. Am. Chem. Soc.* **2010**, *132*, 9715−9727.
(11) Beckwith, M. A.; Roemelt, M.; Collomb, M.-N.; DuBoc, C.; Weng, T.-C.; Bergmann, U.; Glatzel, P.; Neese, F.; DeBeer, S. *Inorg. Chem.* **2011**, *50*, 8397−8409.
(12) Lancaster, K. M.; Finkelstein, K. D.; DeBeer, S. *Inorg. Chem.* **2011**, *50*, 6767−6774.
(13) Bergmann, U.; Glatzel, P. *Photosynth. Res.* **2009**, *102*, 255−266.
(14) Rovezzi, M.; Glatzel, P. *Semicond. Sci. Technol.* **2014**, *29*, 023002.
(15) Rehr, J. J.; Albers, R. C. *Rev. Mod. Phys.* **2000**, *72*, 621−654.
(16) Eeckhout, S. G.; Safonova, O. V.; Smolentsev, G.; Biasioli, M.; Safonov, V. A.; Vykhodtseva, L. N.; Sikora, M.; Glatzel, P. *J. Anal. At. Spectrom.* **2009**, *24*, 215−223.
(17) Safonova, O.; Florea, M.; Bilde, J.; Delichere, P.; Millet, J. *J. Catal.* **2009**, *268*, 156−164.
(18) Safonova, O. V.; Vykhodtseva, L. N.; Polyakov, N. A.; Swarbrick, J. C.; Sikora, M.; Glatzel, P.; Safonov, V. A. *Electrochim. Acta* **2010**, *56*, 145−153.
(19) Smolentsev, G.; Soldatov, A. V.; Messinger, J.; Merz, K.; Weyhermüller, T.; Bergmann, U.; Pushkar, Y.; Yano, J.; Yachandra, V. K.; Glatzel, P. *J. Am. Chem. Soc.* **2009**, *131*, 13161−13167.
(20) Hall, E. R.; Pollock, C. J.; Bendix, J.; Collins, T. J.; Glatzel, P.; DeBeer, S. *J. Am. Chem. Soc.* **2014**, *136*, 10076−10084.
(21) March, A. M.; Assefa, T. A.; Bressler, C.; Doumy, G.; Galler, A.; Gawelda, W.; Kanter, E. P.; Németh, Z.; Pápai, M.; Southworth, S. H.; Young, L.; Vankó, G. *J. Phys. Chem. C* **2015**, *119*, 14571−14578.
(22) Noziéres, P.; de Dominicis, C. T. *Phys. Rev.* **1969**, *178*, 1097−1107.
(23) Schwarz, W. H. E.; Buenker, R. J. *Chem. Phys.* **1976**, *13*, 153−160.
(24) Zhang, Y.; Hua, W.; Bennett, K.; Mukamel, S. In *Density-Functional Methods for Excited States*; Ferré, N., Filatov, M., Huix-Rotllant, M., Eds.; Topics in Current Chemistry; Springer Science + Business Media: 2016; Vol. *368*, pp 273−345.
(25) Hunt, W. J.; Goddard, W. A. *Chem. Phys. Lett.* **1969**, *3*, 414−418.
(26) Ågren, H.; Carravetta, V.; Vahtras, O.; Pettersson, L. G. *Chem. Phys. Lett.* **1994**, *222*, 75−81.
(27) Ågren, H.; Carravetta, V.; Vahtras, O.; Pettersson, L. G. M. *Theor. Chem. Acc.* **1997**, *97*, 14−40.

DOI: 10.1021/acs.jctc.5b00763
J. Chem. Theory Comput. 2015, 11, 5804−5809

(28) Stener, M.; Lisini, A.; Decleva, P. *Chem. Phys.* **1995**, *191*, 141−154.
(29) Triguero, L.; Pettersson, L. G. M.; Ågren, H. *Phys. Rev. B: Condens. Matter Mater. Phys.* **1998**, *58*, 8097−8110.
(30) Prendergast, D.; Galli, G. *Phys. Rev. Lett.* **2006**, *96*, 215502.
(31) Casida, M. E. In *Recent Advances in Density Functional Methods (Part I)*; Chong, D. P., Ed.; World Scientific: 1995; Vol. *1*, Chapter 5, pp 155−192.
(32) Stratmann, R. E.; Scuseria, G. E.; Frisch, M. J. *J. Chem. Phys.* **1998**, *109*, 8218−8224.
(33) Hirata, S.; Head-Gordon, M. *Chem. Phys. Lett.* **1999**, *302*, 375−382.
(34) Zhang, Y.; Healion, D.; Biggs, J. D.; Mukamel, S. *J. Chem. Phys.* **2013**, *138*, 144301.
(35) Wadey, J. D.; Besley, N. A. *J. Chem. Theory Comput.* **2014**, *10*, 4557−4564.
(36) Stener, M.; Fronzoni, G.; de Simone, M. *Chem. Phys. Lett.* **2003**, *373*, 115−123.
(37) Besley, N. A.; Noble, A. *J. Phys. Chem. C* **2007**, *111*, 3333−3340.
(38) DeBeer George, S.; Petrenko, T.; Neese, F. *Inorg. Chim. Acta* **2008**, *361*, 965−972.
(39) Liang, W.; Fischer, S. A.; Frisch, M. J.; Li, X. *J. Chem. Theory Comput.* **2011**, *7*, 3540−3547.
(40) Lopata, K.; Van Kuiken, B. E.; Khalil, M.; Govind, N. *J. Chem. Theory Comput.* **2012**, *8*, 3284−3292.
(41) Zhang, Y.; Biggs, J. D.; Healion, D.; Govind, N.; Mukamel, S. *J. Chem. Phys.* **2012**, *137*, 194306.
(42) Mukamel, S.; Healion, D.; Zhang, Y.; Biggs, J. D. *Annu. Rev. Phys. Chem.* **2013**, *64*, 101−127.
(43) Hirata, S.; Head-Gordon, M. *Chem. Phys. Lett.* **1999**, *314*, 291−299.
(44) Valiev, M.; Bylaska, E. J.; Govind, N.; Kowalski, K.; Straatsma, T. P.; Van Dam, H. J. J.; Wang, D.; Nieplocha, J.; Apra, E.; Windus, T. L.; de Jong, W. A. *Comput. Phys. Commun.* **2010**, *181*, 1477−1489.
(45) Becke, A. D. *J. Chem. Phys.* **1993**, *98*, 5648−5652.
(46) Stephens, P. J.; Devlin, F. J.; Chabalowski, C. F.; Frisch, M. J. *J. Phys. Chem.* **1994**, *98*, 11623−11627.
(47) Weigend, F.; Ahlrichs, R. *Phys. Chem. Chem. Phys.* **2005**, *7*, 3297−3305.
(48) Klamt, A.; Schüürmann, G. *J. Chem. Soc., Perkin Trans. 2* **1993**, 799−805.
(49) Noro, T.; Sekiya, M.; Koga, T. *Theor. Chem. Acc.* **2012**, *131*, 1124.
(50) Krishnan, R.; Binkley, J. S.; Seeger, R.; Pople, J. A. *J. Chem. Phys.* **1980**, *72*, 650−654.
(51) McLean, A. D.; Chandler, G. S. *J. Chem. Phys.* **1980**, *72*, 5639−5648.
(52) Lykos, P. G.; Schmeising, H. N. *J. Chem. Phys.* **1961**, *35*, 288−293.
(53) King, H. F.; Stanton, R. E.; Kim, H.; Wyatt, R. E.; Parr, R. G. *J. Chem. Phys.* **1967**, *47*, 1936−1941.
(54) Casida, M.; Ipatov, A.; Cordova, F. In *Time-Dependent Density Functional Theory*; Marques, M. A., Ullrich, C. A., Nogueira, F., Rubio, A., Burke, K., Gross, E. K. U., Eds.; Lecture Notes in Physics; Springer-Verlag: Berlin, Heidelberg, 2006; Vol. *706*; Chapter 16, pp 243−257.
(55) Ipatov, A.; Cordova, F.; Doriol, L. J.; Casida, M. E. *J. Mol. Struct.: THEOCHEM* **2009**, *914*, 60−73.

DOI: 10.1021/acs.jctc.5b00763
J. Chem. Theory Comput. 2015, 11, 5804−5809